Journal of Science and Technology – Smart Systems and Devices
Volume x, Issue x, Month Year, ppp–ppp

Optimal Conductor Sizing in Active Distribution Networks considering Distributed Generation and Demand Response

Nguyen Thi Anh, Pham Nang Van*
School of Electrical and Electronic Engineering, Hanoi University of Science and Technology, Ha Noi, Vietnam
** Corresponding author email: van.phamnang@hust.edu.vn*

Abstract

Along with the advancement of smart grids and the growing integration of decentralized power generation (DG), distribution networks have experienced significant transformations in topology, operation, and control. In this context, the optimal selection of conductor cross-sections is essential for improving the technical performance and economic efficiency of medium-voltage networks. This study proposes a mathematical framework to determine the optimal selection of conductor cross-sections in distribution networks integrated with DG units and shiftable loads (SLs). The formulated objective function seeks to minimize the overall annual cost, encompassing capital investment, maintenance, energy procurement from the transmission grid, and SL implementation costs, as well as costs associated with DG units. The developed model is modeled as a mixed-integer linear programming (MILP) problem, transformed from a mixed-integer nonlinear programming (MINLP) formulation through the simplified distribution power flow (SD) and linearization techniques. The model is tested on the IEEE 33-node test feeder under three distinct scenarios. Simulations are performed using the GUROBI solver within the GAMS platform. The results highlight the substantial impact of DG and SL integration on conductor sizing and the overall operational costs of distribution networks.

Keywords: Distributed generation (DG), mixed-integer linear programming (MILP), optimal conductor size, shiftable load (SL).

1. Introduction

Conductor sizing is a crucial task in power system planning. An appropriate conductor size not only ensures the safe operation of the power system but also optimizes maintenance, power loss, and energy loss costs.

The problem of determining conductor sizes has been addressed in several research papers. In [1], a method developed using a genetic algorithm (GA) was proposed to determine conductor size, locations, and capacities of shunt capacitors installed in distribution networks in order to minimize overall investment and operating expenditures while considering harmonics in the power system. Study [2] developed a procedure for calculating conductor cross-sections based on steady-state analysis to decrease active power losses while improving voltage quality. A simple procedure for determining cable sizes with rated voltages below 1000 V to mitigate the thermal aging of cable insulation was proposed in [3]. A drawback of studies [2–3] is that the conductor sizing problem was not formulated as an explicit mathematical optimization model; therefore, the obtained solutions are often locally optimal.

The authors in [4] presented a mixed-integer linear programming (MILP) optimization model for determining conductor sizes for both new investment and network reinforcement cases. The MILP model in [4] was converted from a mixed-integer nonlinear programming (MINLP) model through a piecewise linearization approach. Study [5] developed a procedure based on the economic current density range and heuristic methods to calculate conductor cross-sections. Although the conductor sizing technique in [5] does not require complex optimization algorithms and is easy to understand and implement, it often fails to obtain the global optimal solution.

The metaheuristic NSIHSA-II was developed in [6] to determine solutions for a multi-objective optimization model in distribution network investment strategies with integrated renewable and distributed generation (DG) sources. In [7], the SSO metaheuristic was utilized to determine optimal conductor sizes for both new investment and renovation projects in Egypt, while facilitating high integration of distributed generation. In [7], a feeder reinforcement index (FRI) was developed to identify the lines requiring upgrades, thereby significantly reducing the search space and computational time.

Paper [8] developed an MINLP optimization model for the optimal conductor sizing problem, simultaneously determining the optimal locations and capacities of shunt capacitors. This proposed optimization model considers variations in load power demand with respect to voltage, while the locations and costs of shunt capacitors are accurately modeled using integer variables. Similarly, the authors in [9] formulated an MINLP optimization

p-ISSN 3093-3285
e-ISSN 3093-3315
https://doi.org/10.51316/jst.xxx.ssad.xxxx.xx.x.x
Received: Feb 2, 2026; Revised: Apr 21, 2026;
Accepted: May 22, 2026; Online: Jul 1, 2026

model and applied the nonlinear optimization solver DICOPT within the GAMS environment to determine conductor sizes. A metaheuristic harmony search algorithm (HSA) was developed in [10] to determine optimal conductor sizes. Paper [11] proposed a mixed-integer quadratically constrained programming (MIQCP) model to compute the optimal conductor cross-section. Paper [12] proposed a mixed-integer second-order cone programming (MISOCP) framework for optimal selection of conductor cross-sections, uniquely integrating daily consumption patterns and voltage-dependent load models to ensure a globally optimal solution. Work [13] introduced a novel leader-follower optimization methodology based on the Chu & Beasley Genetic Algorithm (CBGA) to simultaneously address conductor selection and phase balancing in unbalanced distribution networks, demonstrating superior performance in minimizing total costs and processing times compared to other metaheuristic techniques. Study [14] proposed an adaptive robust optimization framework using the Column and Constraint Generation algorithm for the conductor size selection problem in radial distribution systems, providing a computationally efficient solution that ensures operational reliability under worst-case demand scenarios driven by electric vehicles and distributed generation. Work [15] proposed a novel MILP framework to simultaneously address distribution network reconfiguration and conductor selection, demonstrating that this integrated approach achieves superior power loss reduction and voltage profile enhancement while ensuring global optimality compared to traditional sequential or standalone methods.

From studies [1−15], it can be observed that the optimal conductor sizing problem is commonly addressed by applying optimization approaches such as MINLP, MIQCP, MILP, MISOCP, and metaheuristic techniques. However, these studies typically perform calculations at a single peak load condition and assume fixed load power consumption. In addition, conductor sizing is often carried out for distribution networks without distributed generation. The main goal of this paper is to evaluate the impact of distributed generation and shiftable loads (SLs) on optimal conductor sizing using a mixed-integer linear programming (MILP) approach that accounts for time-varying load power consumption. This framework is developed as a strategic offline planning tool for a Distribution System Operator (DSO), providing a clear context for the assumptions made regarding bidding structures and cost parameters. The key contributions of this study are summarized as follows:

- Addressing the conductor sizing challenge in distribution networks from the DSO’s perspective, in which the objective function is formulated to minimize the total annual expense of the distribution network. This cost includes capital investment and maintenance costs for the lines, electricity trading cost with the transmission grid, electricity purchase costs from distributed generators (DGs), and costs associated with load adjustments. The model also adheres to constraints regarding nodal voltage limits, power exchange limits with the transmission grid, and bounds on load flexibility.
- Transforming the original MINLP model into a MILP model based on the Simplified DistFlow (SD) model, linearization techniques for products of binary and continuous variables, and a linearization approach for branch power flow limits using a 12-sided regular polygon;
- Applying the proposed MILP model to derive the optimal conductor cross-sections for the IEEE 33-node medium-voltage distribution network under three different scenarios.

The remainder of this paper includes three sections. Section 2 describes the MINLP and MILP models for conductor size selection problem in distribution networks along with distributed generation and controllable loads with time-varying power consumption. Section 3 presents the optimization results and discussion for the IEEE 33-node medium-voltage distribution network. Conclusions and future research directions are provided in Section 4.

2. Materials and Methods

2.1. Mixed-Integer Nonlinear Programming Model

The objective function and constraints for the conductor size optimization problem in distribution networks, incorporating DG and SL with time-varying power consumption, are formulated as follows.

2.1.1. Objective function

The objective function (1) of the optimization model is to achieve the minimum total annualized cost of the distribution network. This objective function consists of four components:

- f_1 is the overall investment and maintenance expenditure of lines;
- f_2 is the expense of energy trading with the transmission network;
- f_3 is the cost of purchasing electricity from DG units;
- f_4 is the adjustment cost of loads.

$$\min\left(f_1 + f_2 + f_3 + f_4\right) \tag{1}$$

$$f_1 = \left(\begin{array}{l} \sum\limits_{ij\in\Omega_{\mathrm{L}}}\sum\limits_{k\in\Omega_{\mathrm{S}}} K_{0,k}\times u_{ij,k}\times L_{ij}\times\dfrac{r\left(1+r\right)^N}{\left(1+r\right)^N-1} \\ +\sum\limits_{ij\in\Omega_{\mathrm{L}}}\sum\limits_{k\in\Omega_{\mathrm{S}}} K_{0,k}\times u_{ij,k}\times L_{ij}\times a_{\mathrm{mc}} \end{array}\right) \tag{2}$$

$$f_2 = 365\times\sum_{t=1}^{T}\sum_{i\in\Omega_{\mathrm{sub}}} c_{i.t}^{\mathrm{sub}}\times P_{i,t}^{\mathrm{sub}}\times S_{\mathrm{base}} \tag{3}$$

$$f_3 = 365\times\sum_{t=1}^{T}\sum_{b=1}^{\mathrm{N_{DG\mathit{i}}}}\sum_{i\in\Omega_{\mathrm{DG}}}\lambda_{ib}^{\mathrm{DG}}\times P_{ib,t}^{\mathrm{DG}}\times S_{\mathrm{base}} \tag{4}$$

$$f_4 = 365\times\sum_{t=1}^{T}\sum_{i\in\Omega_{\mathrm{SL}}}\left(c_{i,t}^{\mathrm{D+}}\alpha_{i,t}^{+}+c_{i,t}^{\mathrm{D-}}\alpha_{i,t}^{-}\right)\times P_{i,t}^{\mathrm{SL,0}}\times S_{\mathrm{base}} \tag{5}$$

where:

- Ω_{L} represents the set of branches;
- Ω_{S} represents the set of available standard conductor types;
- Ω_{DG} represents the set of buses where DG units are installed;
- Ω_{sub} represents the set of substation nodes in the distribution network;
- Ω_{SL} represents the set of nodes with shiftable loads;
- S_{base} represents the system base power(kVA);
- r represents the discount rate;
- a_{mc} is the maintenance cost coefficient;
- N is the operational lifetime of the conductors (years);
- $K_{0,k}$ is the investment expense per unit length for conductor type k ($/km);
- L_{ij} is the length of line branch ij (km);
- $c_{i.t}^{\mathrm{sub}}$ is the electricity price purchased from the transmission grid at substation node i at time t ($/MWh);
- $P_{i,t}^{\mathrm{sub}}$ represents the power imported from the transmission grid at substation bus i at time t (p.u.);
- λ_{ib} is the bidding price corresponding to block b of the DG unit at bus i ($/MWh);
- $P_{ib,t}^{\mathrm{DG}}$ is the generated power corresponding to block b of the DG unit at bus i at time t (p.u.);
- $\alpha_{i,t}^{+}$ and $\alpha_{i,t}^{-}$ are the percentages of upward and downward power adjustment of the controllable load, respectively;
- $c_{i,t}^{\mathrm{D+}}$ and $c_{i,t}^{\mathrm{D-}}$ are the upward and downward adjustment costs of the controllable load at node i during time interval t ($/MWh);
- $P_{i,t}^{\mathrm{SL,0}}$ is the initial power consumption of the controllable load at bus i during time interval t (p.u.);
- $u_{ij,k}$ is a binary variable, where $u_{ij,k}=1$ if line ij uses conductor type k, and $u_{ij,k}=0$ otherwise;
- T is the overall number of operational scheduling time periods (where $T = 24$).

It is noted that, regarding the pre-existing infrastructure, the proposed model handles existing branches by pre-assigning the binary variable $u_{ij,k}$ = 1 for the conductor type k that is currently in place on branch ij. For these specific branches, the associated investment cost in the objective function is set to zero. However, the model maintains flexibility by allowing the optimization process to trigger a reinforcement (i.e., selecting a larger cross-section) if an upgrade is required to satisfy technical constraints or enhance economic efficiency.

Furthermore, it should be noted that this study focuses on the DSO's economic planning and operational procurement. It is assumed that the DG units and the infrastructure for shiftable loads are owned and operated by third-party entities (e.g., independent power producers or prosumers). Therefore, their capital investments are not included in the DSO's annualized cost (f_1). Instead, the DSO incentivizes these entities through electricity purchase prices (f_3) and load adjustment compensations (f_4), which are assumed to reflect market rates that allow third-party recovery of their investments.

2.1.2. Constraints of shiftable loads

Let $\left[F_{i,t}^{-},F_{i,t}^{+}\right]$ be the flexibility range of the controllable load at bus i during time interval t. This flexibility range is defined as being near 1, such that $0\le F_{i,t}^{-}\le 1$ and $F_{i,t}^{+}\ge 1$. If the load at node i is non-adjustable then $F_{i,t}^{-}=F_{i,t}^{+}=1$. The model for controllable loads is described by constraints (6)–(11).

$$P_{i,t}^{\mathrm{SL}}=\alpha_{i,t}P_{i,t}^{\mathrm{SL,0}};\ \forall i\in\Omega_{\mathrm{SL}};t=1,...,T \tag{6}$$

$$Q_{i,t}^{\mathrm{SL}}=P_{i,t}^{\mathrm{SL}}\left[\tan\left(\arccos\varphi_i^{\mathrm{SL}}\right)\right];\ \forall i\in\Omega_{\mathrm{SL}};t=1,...,T \tag{7}$$

$$\alpha_{i,t}=1+\alpha_{i,t}^{+}-\alpha_{i,t}^{-};\ \forall i\in\Omega_{\mathrm{SL}};t=1,...,T \tag{8}$$

$$0\le\alpha_{i,t}^{+}\le F_{i,t}^{+}-1;\ \forall i\in\Omega_{\mathrm{SL}};t=1,...,T \tag{9}$$

$$0\le\alpha_{i,t}^{-}\le 1-F_{i,t}^{-};\ \forall i\in\Omega_{\mathrm{SL}};t=1,...,T \tag{10}$$

$$\sum_{t=1}^{T}P_{i,t}^{\mathrm{SL}}=\sum_{t=1}^{T}P_{i,t}^{\mathrm{SL,0}};\ \forall i\in\Omega_{\mathrm{SL}} \tag{11}$$

in which:

- Ω_{SL} is the set of nodes linked to shiftable loads;

- $P_{i,t}^{\mathrm{SL}}$ and $Q_{i,t}^{\mathrm{SL}}$ are the real and reactive power demand of the shiftable load at bus *i* during time interval *t* (p.u.);
- $\cos\varphi_i^{\mathrm{SL}}$ is the power factor of the shiftable load, which is determined from the initial power factor and is assumed to remain constant;
- $P_{i,t}^{\mathrm{SL,0}}$ is the initial active power consumption of the shiftable load at node *i* during time interval *t* (p.u.);
- $\alpha_{i,t}$ represents the percentage of power change for the shiftable load at bus *i* during time interval *t*;
- $F_{i,t}^{+}$ and $F_{i,t}^{-}$ are the upper and lower limits for power consumption adjustment of the controllable load at node *i* during time interval *t*;

Constraints (6) and (7) describe the real and reactive power demand of the controllable load at node *i* during time interval *t*. The load adjustment factor is presented in equation (8). The expressions $\left(F_{i,t}^{+}-1\right)$ and $\left(1-F_{i,t}^{-}\right)$ are proportional to the load in the upward and downward adjustment directions, respectively, as modeled in constraints (9) and (10). Finally, constraint (11) guarantees that the total real power consumption of the flexible load remains constant over the entire scheduling period *T*.

2.1.3. Constraints of distributed generation units

The decentralized power generation model, featuring a multi-block bidding structure, is presented in constraints (12)–(15).

$$0 \le P_{ib,t}^{\mathrm{DG}} \le P_{ib,t}^{\mathrm{DG,max}} \; ;\forall i \in \Omega_{\mathrm{DG}}, \forall b \in \mathrm{N}_{\mathrm{DG}i}, t = 1,\ldots,T \quad (12)$$

$$P_{i,t}^{\mathrm{DG}} = \sum_{b=1}^{\mathrm{N}_{\mathrm{DG}i}} P_{ib,t}^{\mathrm{DG}} \; ; \; \forall i \in \Omega_{\mathrm{DG}}, t = 1,\ldots,T \quad (13)$$

$$P_{i,t}^{\mathrm{DG,min}} \le P_{i,t}^{\mathrm{DG}} \le P_{i,t}^{\mathrm{DG,max}} \; ;\forall i \in \Omega_{\mathrm{DG}}, \; t = 1,\ldots,T \quad (14)$$

$$Q_{i,t}^{\mathrm{DG}} = P_{i,t}^{\mathrm{DG}} \times \tan\left(\arccos\varphi_i^{\mathrm{DG}}\right); \; \forall i \in \Omega_{\mathrm{DG}}; t = 1,...,T \quad (15)$$

where:

- Ω_{DG} represents the set of buses where DG units are installed;
- $P_{ib,t}^{\mathrm{DG,max}}$ is the maximum generating power of block *b* corresponding to the DG unit at bus *i* at time *t* (p.u.);
- $P_{i,t}^{\mathrm{DG}}$ and $Q_{i,t}^{\mathrm{DG}}$ are the active and reactive generated power of the DG unit at bus *i* at time *t* (p.u.);
- $P_{i,t}^{\mathrm{DG,max}}$ and $P_{i,t}^{\mathrm{DG,min}}$ are the upper and lower bounds of power output of the DG unit at node *i* at time *t* (p.u.), respectively;
- $\cos\varphi_i^{\mathrm{DG}}$ is the operating power factor at the interconnection point of the DG unit at node *i*;

Contraint (12) enforces the generated power limits for each individual bidding block of the DG units. Contraint (13) characterizes the overall power generation of the DG units at time interval *t*. The active power output of the DG units is restricted by (14). Equation (15) is employed to describe their reactive power output.

It is noted that the multi-block bidding structure for DGs represents a realistic local electricity market where different generation units (or the same unit at different output levels) offer electricity at varying marginal costs. This bidding mechanism interacts dynamically with the grid purchase price ($c_{i.t}^{\mathrm{sub}}$). Specifically, when DG bidding prices are lower than $c_{i.t}^{\mathrm{sub}}$, the DSO prioritizes local generation, which reduces the power flow imported from the transmission grid and potentially leads to smaller optimal conductor sizes for the main feeders. Conversely, if DG bids are uncompetitive, the system relies more on the upstream grid, necessitating larger conductors to handle the increased load. This economic trade-off is a key driver in the sizing optimization process.

2.1.4. Constraints of the power network

The constraints of the distribution network are modeled as follows:

$$P_{i,t}^{\mathrm{sub}} \ge 0 \; ;\forall i \in \Omega_{\mathrm{sub}}; \; t = 1,\ldots,T \quad (16)$$

$$P_{i,t}^{\mathrm{sub}} + P_{i,t}^{\mathrm{DG}} - P_{i,t}^{\mathrm{D}} - P_{i,t}^{\mathrm{SL}} = \left(\begin{array}{l} \sum\limits_{\forall k \in \Omega_{\mathrm{S}}} \sum\limits_{j \in \Omega_i, j \ne h} u_{ij,k} P_{ij,k,t} \\ - \sum\limits_{\forall k \in \Omega_{\mathrm{S}}} u_{hi,k} \left(P_{hi,k,t} - \dfrac{P_{hi,k,t}^2 + Q_{hi,k,t}^2}{U_{h,t}^2} R_{0,k} L_{ij} \right) \end{array} \right); \quad (17)$$

$$\forall i \in \Omega_{\mathrm{N}}; \; t = 1,\ldots,T$$

$$Q_{i,t}^{\mathrm{sub}} + Q_{i,t}^{\mathrm{DG}} - Q_{i,t}^{\mathrm{D}} - Q_{i,t}^{\mathrm{SL}} = \left(\begin{array}{l} \sum\limits_{\forall k \in \Omega_{\mathrm{S}}} \sum\limits_{j \in \Omega_i, j \ne h} u_{ij,k} Q_{ij,k,t} \\ - \sum\limits_{\forall k \in \Omega_{\mathrm{S}}} u_{hi,k} \left(Q_{hi,k,t} - \dfrac{P_{hi,k,t}^2 + Q_{hi,k,t}^2}{U_{h,t}^2} X_{0,k} L_{ij} \right) \end{array} \right); \quad (18)$$

$$\forall i \in \Omega_{\mathrm{N}}; \; t = 1,\ldots,T$$

$$\left(\begin{array}{l} U_{i,t}^2 - U_{j,t}^2 \\ -2 \times L_{ij} \times \sum\limits_{k \in \Omega_{\mathrm{S}}} u_{ij,k} \times \left(R_{0,k} P_{ij,k,t} + X_{0,k} Q_{ij,k,t} \right) \\ + \sum\limits_{k \in \Omega_{\mathrm{S}}} u_{ij,k} \times \left[\left(L_{ij} R_{0,k} \right)^2 + \left(L_{ij} X_{0,k} \right)^2 \right] \\ \times \dfrac{P_{ij,k,t}^2 + Q_{ij,k,t}^2}{U_{i,t}^2} \end{array} \right) = 0; \quad (19)$$

$$\forall ij \in \Omega_{\mathrm{L}}; \; t = 1,\ldots,T$$

$$U_{i,\min} \le U_{i,t} \le U_{i,\max}; \; \forall i \in \Omega_{\mathrm{N}} \setminus \{i = 1\}; \; t = 1,\ldots,T \quad (20)$$

$$U_{1,t} = U_0 \; ; t = 1,\ldots,T \tag{21}$$

$$\sum_{k\in\Omega_S}\left(P_{ij,k,t}u_{ij,k}\right)^2 + \sum_{k\in\Omega_S}\left(Q_{ij,k,t}u_{ij,k}\right)^2 \le \sum_{k\in\Omega_S}\left(S_{ij,k}^{\max}u_{ij,k}\right)^2 ; \forall ij\in\Omega_L ;\; t=1,\ldots,T \tag{22}$$

$$\sum_{ij\in\Omega_L}\sum_{k\in\Omega_S} K_{0,k}\times u_{ij,k}\times L_{ij} \le K \tag{23}$$

$$\sum_{k\in\Omega_S} u_{ij,k} = 1;\; \forall ij\in\Omega_L \tag{24}$$

$$u_{ij,k}\in\{0,1\};\; \forall ij\in\Omega_L;\; \forall k\in\Omega_S \tag{25}$$

where:

- Ω_i represents the set of buses connected directly to bus *i*;
- Ω_N is the set of all nodes in the network;
- K is the investment budget ($);
- $P_{ij,t}$ is the real power flowing through section *ij* at time *t* (p.u.);
- $P_{ij,k,t}$ is the real power flowing through section *ij* with conductor type *k* at interval *t* (p.u.);
- $Q_{ij,t}$ is the reactive power flowing through section *ij* at time *t* (p.u.);
- $Q_{ij,k,t}$ is the reactive power flowing through section *ij* with conductor type *k* at time interval *t* (p.u.);
- $R_{0,k}$ is the unit resistance of conductor type *k* (p.u./km);
- $X_{0,k}$ is the unit reactance of conductor type *k* (p.u./km);
- $Q_{i,t}^{\text{sub}}$ is the reactive power exchanged with the transmission grid at substation bus *i* at time *t* (p.u.);
- $P_{i,t}^{\text{D}}, Q_{i,t}^{\text{D}}$ are the real and reactive power of non-controllable loads at node *i* at time *t* (p.u.), respectively;
- $U_{i,t}$ is the voltage at bus *i* at time *t* (p.u.);
- $U_{i,\min}$ and $U_{i,\max}$ are the upper and lower bounds of voltage at node *i* (p.u.), respectively;

Constraint (16) specifies that the distribution network only purchases electricity supplied by the transmission network. Constraints (17) and (18) represent the power balance equations utilizing the branch flow equations for radial distribution networks. Equation (19) expresses the voltage relation between nodes of section *ij*. Equation (20) defines the nodal voltage limits. Constraint (21) specifies the substation node voltage (node 1) at time interval *t.* Equation (22) describes the power transfer capacity limits of the lines. Constraint (23) represents the total investment budget limit. Constraint (24) ensures that each line branch is assigned only one conductor cross-section type. Finally, constraint (25) describes the binary variables.

2.2. Mixed-integer Linear Programming Model

2.2.1. Simplified power flow model of the power network

The grid model described in Section 2.1 is an inherently non-linear problem (MINLP) due to the power flow equations (17)–(19) and the line capacity constraint (22). The linearization technique for these constraints is presented below.

Under normal operating conditions, power losses on the distribution lines are typically significantly smaller than the branch power flow [16]. Consequently, the branch power loss component can be neglected. Furthermore, nodal voltage magnitudes are generally approximated to 1.0 pu [17].

$$\left(U_i - 1\right)^2 = U_i^2 - 2U_i + 1 \approx 0 \tag{26}$$

Substituting (26) into (19), the expression (27) is obtained:

$$\begin{pmatrix} U_{i,t} - U_{j,t} - L_{ij} \\ \times\sum_{k\in\Omega_S} u_{ij,k}\times\left(R_{0,k}P_{ij,k,t} + X_{0,k}Q_{ij,k,t}\right) \end{pmatrix} = 0; \quad \forall ij\in\Omega_L;\; t=1,\ldots,T \tag{27}$$

Consequently, the simplified power flow model for the distribution network is described as follows:

$$P_{i,t}^{\text{sub}} + P_{i,t}^{\text{DG}} - P_{i,t}^{\text{D}} - P_{i,t}^{\text{SL}} = \sum_{\forall k\in\Omega_S}\sum_{j\in\Omega_i, j\neq h} u_{ij,k}P_{ij,k,t} - \sum_{\forall k\in\Omega_S} u_{hi,k}P_{hi,k,t} \; ; \quad \forall i\in\Omega_N;\; t=1,\ldots,T \tag{28}$$

$$Q_{i,t}^{\text{sub}} + Q_{i,t}^{\text{DG}} - Q_{i,t}^{\text{D}} - Q_{i,t}^{\text{SL}} = \sum_{\forall k\in\Omega_S}\sum_{j\in\Omega_i, j\neq h} u_{ij,k}Q_{ij,k,t} - \sum_{\forall k\in\Omega_S} u_{hi,k}Q_{hi,k,t} ; \quad \forall i\in\Omega_N;\; t=1,\ldots,T \tag{29}$$

The linearization of constraint (22) using a regular polygon approximation [18] yields the following formulation in (30):

$$\sum_{k\in\Omega_S} k_c^{(1)}P_{ij,k,t}u_{ij,k} + \sum_{k\in\Omega_S} k_c^{(2)}Q_{ij,k,t}u_{ij,k} + \sum_{k\in\Omega_S} k_c^{(3)}S_{ij,k}^{\max}u_{ij,k} \le 0 \; ; \forall ij\in\Omega_L ; \quad c=1,\ldots,12;\; t=1,\ldots,T \tag{30}$$

in which, $k_c^{(1)}, k_c^{(2)}$ and $k_c^{(3)}$ are the linearization coefficients determined according to [18].

It is emphasized that while the SD model introduces certain simplifications by neglecting power losses and assuming nodal voltages near 1.0 pu, these assumptions are widely accepted in strategic distribution planning. According to [19], the error margins introduced by the SD model compared to full non-linear AC power flow (e.g., Newton-Raphson) remain within an acceptable range for conductor sizing and network expansion problems. Furthermore, the use of the SD model to ensure global optimality and computational tractability is a well-established practice in recent literature, as demonstrated in [20] and related studies.

2.2.2. Linearization of the product of binary and continuous variables

Constraints (27)–(30) are nonlinear since they consist of multiplying binary and continuous variables. Because of this, these elements are transformed into linear form via the following transformation steps:

Let :

$$\tilde{P}_{ij,k,t} = u_{ij,k} P_{ij,k,t};\ \tilde{Q}_{ij,k,t} = u_{ij,k} Q_{ij,k,t} \tag{31}$$

hence:

$$\tilde{P}_{ij,k,t} = \begin{cases} 0 & \text{if } u_{ij,k} = 0 \\ P_{ij,k,t} & \text{if } u_{ij,k} = 1 \end{cases} \quad \text{and } \tilde{Q}_{ij,k,t} = \begin{cases} 0 & \text{if } u_{ij,k} = 0 \\ Q_{ij,k,t} & \text{if } u_{ij,k} = 1 \end{cases} \tag{32}$$

The linear components $\tilde{P}_{ij,k,t}$ and $\tilde{Q}_{ij,k,t}$ are formualted in constraints (33)-(38).

$$\tilde{P}_{ij,k,t} = P_{ij,k,t} - y_{ij,k};\ \forall ij \in \Omega_{\mathrm{L}};\ \forall k \in \Omega_{\mathrm{S}};\ t = 1,\ldots,T \tag{33}$$

$$-M \times u_{ij,k} \le \tilde{P}_{ij,k,t} \le M \times u_{ij,k};\ \forall ij \in \Omega_{\mathrm{L}};\ \forall k \in \Omega_{\mathrm{S}};\ t = 1,\ldots,T \tag{34}$$

$$-M \times \left(1 - u_{ij,k}\right) \le y_{ij,k} \le M \times \left(1 - u_{ij,k}\right);\ \forall ij \in \Omega_{\mathrm{L}};\ \forall k \in \Omega_{\mathrm{S}} \tag{35}$$

$$\tilde{Q}_{ij,k,t} = Q_{ij,k,t} - z_{ij,k};\ \forall ij \in \Omega_{\mathrm{L}};\ \forall k \in \Omega_{\mathrm{S}};\ t = 1,\ldots,T \tag{36}$$

$$-M \times u_{ij,k} \le \tilde{Q}_{ij,k,t} \le M \times u_{ij,k};\ \forall ij \in \Omega_{\mathrm{L}};\ \forall k \in \Omega_{\mathrm{S}};\ t = 1,\ldots,T \tag{37}$$

$$-M \times \left(1 - u_{ij,k}\right) \le z_{ij,k} \le M \times \left(1 - u_{ij,k}\right);\ \forall ij \in \Omega_{\mathrm{L}};\ \forall k \in \Omega_{\mathrm{S}} \tag{38}$$

where, $y_{ij,k}$ and $z_{ij,k}$ are auxiliary variables; M is a sufficiently large positive constant.

Specifically, the non-linear constraints (27)–(30) are converted into the following linear constraints:

$$\begin{pmatrix} U_{i,t} - U_{j,t} - L_{ij} \\ \times \sum_{k \in \Omega_{\mathrm{S}}} \left(R_{0,k} \tilde{P}_{ij,k,t} + X_{0,k} \tilde{Q}_{ij,k,t} \right) \end{pmatrix} = 0;\ \forall ij \in \Omega_{\mathrm{L}};\ t = 1,\ldots,T \tag{39}$$

$$P_{i,t}^{\mathrm{sub}} + P_{i,t}^{\mathrm{DG}} - P_{i,t}^{\mathrm{D}} - P_{i,t}^{\mathrm{SL}} = \sum_{\forall k \in \Omega_{\mathrm{S}}} \sum_{j \in \Omega_i, j \ne h} \tilde{P}_{ij,k,t} - \sum_{\forall k \in \Omega_{\mathrm{S}}} \tilde{P}_{hi,k,t};\ \forall i \in \Omega_{\mathrm{N}};\ t = 1,\ldots,T \tag{40}$$

$$Q_{i,t}^{\mathrm{sub}} + Q_{i,t}^{\mathrm{DG}} - Q_{i,t}^{\mathrm{D}} - Q_{i,t}^{\mathrm{SL}} = \sum_{\forall k \in \Omega_{\mathrm{S}}} \sum_{j \in \Omega_i, j \ne h} \tilde{Q}_{ij,k,t} - \sum_{\forall k \in \Omega_{\mathrm{S}}} \tilde{Q}_{hi,k,t};\ \forall i \in \Omega_{\mathrm{N}};\ t = 1,\ldots,T \tag{41}$$

$$\begin{pmatrix} \sum_{k \in \Omega_{\mathrm{S}}} k_c^{(1)} \tilde{P}_{ij,k,t} + \sum_{k \in \Omega_{\mathrm{S}}} k_c^{(2)} \tilde{Q}_{ij,k,t} \\ + \sum_{k \in \Omega_{\mathrm{S}}} k_c^{(3)} S_{ij,k}^{\max} u_{ij,k} \end{pmatrix} \le 0;\ \forall ij \in \Omega_{\mathrm{L}};\ c = 1,\ldots,12;\ t = 1,\ldots,T \tag{42}$$

2.2.3. MILP-based formulation

The mixed-integer linear programming model for the optimal selection of conductor sizes problem in distribution networks, incorporating distributed generation and controllable loads, is formulated as follows:

The objective function: (1).

Satisfying the following sets of constraints:

- Controllable load constraints: (6)–(11);
- Decentralized power generation constraints: (12)–(15);
- Linearized grid constraints: (16), (20)–(21), (23)–(25), (33)–(42).

3. Results and Discussions

In this section, the developed optimal approach is used to calculate the modified IEEE 33-bus medium-voltage distribution system [21]. The simulation is implemented in the GAMS programming environment [22] utilizing the GUROBI commercial solver. All computations are performed on a personal computer equipped with an AMD Ryzen 5 5600G 3.9 GHz processor and 32 GB of RAM. The operating voltage at the substation (bus 1) is set to 1.0 per unit. Fig. 1 illustrates the flowchart of the proposed optimization framework.

3.1. Description of Power Network Data

The single-line diagram of the modified IEEE 33-bus medium-voltage distribution system is shown in Fig. 2. The nominal voltage of the network is 12.66 kV. The overall peak load demand is 7355 + *j*6239.05 kVA. The required voltage limits are $0.94 \le U \le 1.06$ per unit. The base values are S_{cb} = 1000 kVA and U_{cb} = 12.66 kV. The load characteristics at the buses [25] are provided in Table 1. Fig. 3 illustrates the daily power consumption variations for three load types (residential, commercial, and industrial) [26] corresponding to three distinct daily load profiles. In Fig. 3, the time-varying power consumption is expressed as a percentage of the maximum load. Fig. 4 describes the electricity purchasing price at the Point of Common Coupling [27]. Furthermore, 29 types of conductors (denoted as k1 to k29) [23] are utilized in this study. The operational lifetime of the conductors is assumed to be 20 years, with a discount rate of 7% and a maintenance factor of 2%.

The technical parameters of the DG units are listed in Table 2. The three-block bidding data of the DGs are presented in Table 3.

Parameters and Locations of SLs [24]: The adjustable loads are located at buses 8, 14, 24, 25, and 30. The adjustment limits are expressed as: $\left[F_{i,t}^{-}, F_{i,t}^{+}\right] = [0.5; 1.5]$. The costs for increasing and decreasing load demand are 3 \$/MWh.

3.2. Numerical Results

In this study, three scenarios of load profiles are evaluated and compared, including:

− **Scenario 1**: The network without distributed generation but with adjustable loads;

− **Scenario 2**: The network with distributed generation but without adjustable loads;

− **Scenario 3**: The network with both distributed generation and adjustable loads. The calculated results of the objective function and other quantities corresponding to the scenarios are provided in Table 4.

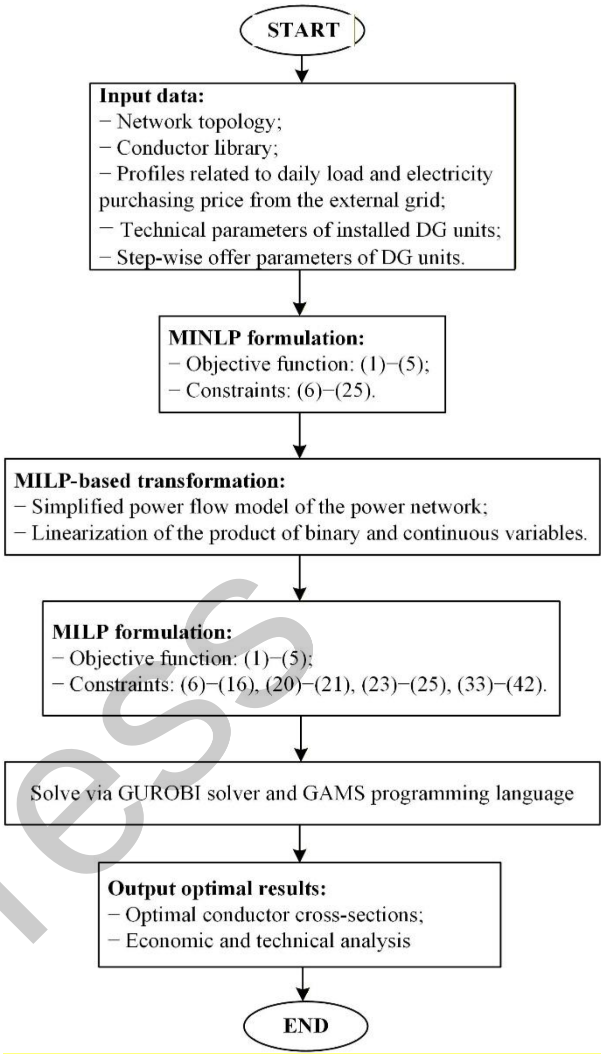

Fig. 1. Flowchart of the proposed optimization framework

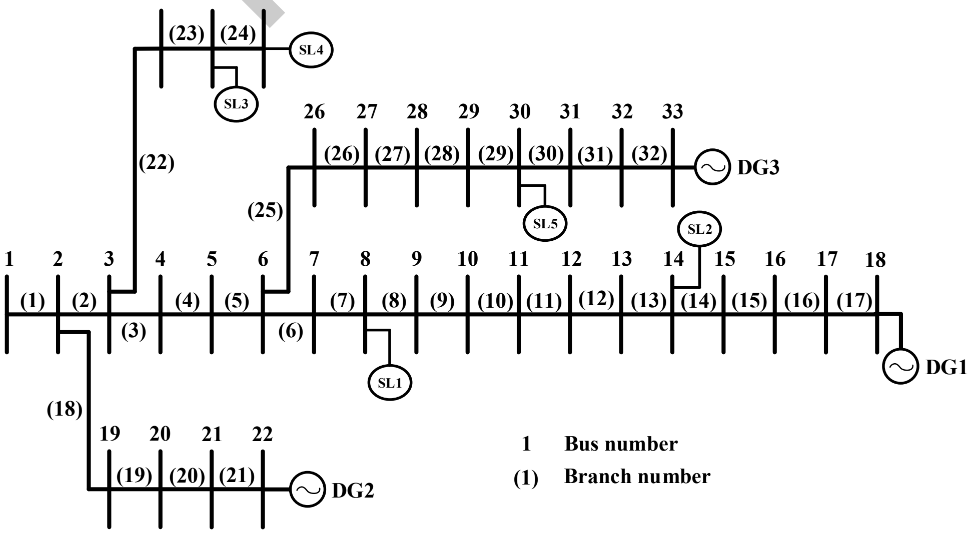

Fig. 2. Modified IEEE 33-bus medium-voltage

Journal of Science and Technology − Smart Systems and Devices
Volume x, Issue x, Month Year, ppp–ppp

Table 1. Load specifications

Load type	**Bus**
Residential	2, 5, 12, 14, 19, 22, 31, 32
Commercial	4, 7, 8, 10, 11, 13, 15, 17, 20, 23, 24, 25, 26, 28, 29, 30, 33
Industrial	3, 6, 9, 16, 18, 21, 27

Table 2. Technical parameters of installed DG units

DG unit	**Location (Bus)**	$P_i^{\mathrm{DG,min}}\ (\mathrm{kW})$	$P_i^{\mathrm{DG,max}}\ (\mathrm{kW})$	$\cos\varphi^{\mathrm{DG}}$
DG1	18	0	2000	0.9
DG2	22	0	1700	
DG3	23	0	1500	

Table 3. Step-wise offer parameters of DG units

DG unit	**Block segment**	**Block size (kW)**	**Bid price ($/kWh)**
DG1	1	700	0.006
	2	700	0.008
	3	600	0.012
DG2	1	600	0.007
	2	400	0.009
	3	700	0.013
DG3	1	800	0.007
	2	200	0.014
	3	500	0.020

Table 4. Comparison of optimization results among the three scenarios

Description	**Scenario**		
	1	2	3
Minimum voltage (p.u.)	0.9400	0.9485	0.9423
Maximum voltage (p.u.)	1.0000	1.0600	1.0600
Annualized conductor investment cost ($/year)	889.46	441.62	448.65
Annual conductor maintenance cost ($/year)	188.46	93.57	95.06
Power purchasing cost from the external grid ($/year)	741,625.58	97,291.00	26,330.55
Power purchasing cost from the DGs ($/year)	0	315,749.09	328,622.29
Load adjustment cost ($/year)	30,545.44	0	19,139.63
Total annual cost ($/year)	773,248.94	413,575.27	374,636.18

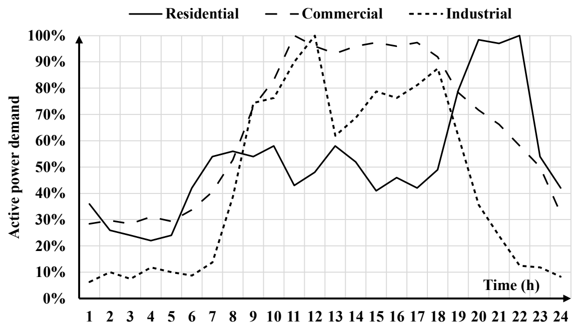

Fig. 3. Daily load profile

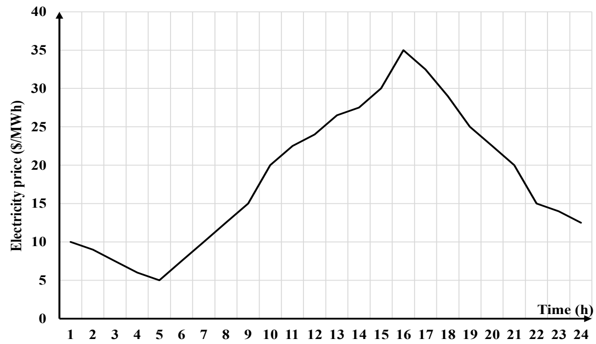

Fig. 4. Electricity purchasing price from the external grid

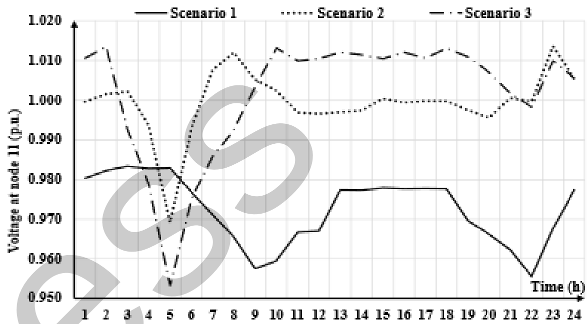

Fig. 5. Voltage profile at bus 11

Table 4 illustrates significant variations among the three scenarios with respect to voltage profiles and economic indicators. While the minimum voltage magnitudes show slight differences across the scenarios, these values occur at different buses and time steps. Specifically, in Scenario 1, the lowest voltage is 0.94 p.u. (at node 18, $t = 22$). In Scenario 2, the lowest voltage is observed at node 25 at $t = 11$. In Scenario 3, it occurs at bus 33 at $t = 5$. In contrast, the maximum voltage levels differ significantly. For Scenario 1, the maximum voltage remains at 1.00 per unit. However, integrating DGs in Scenarios 2 and 3 raises the maximum voltage to 1.06 p.u. (at bus 18, $t = 23$), which is at the upper limit of the permissible range, indicating the active power injection support from DG units.

Economically, Scenario 3 is the most optimal solution, achieving the lowest total annual cost of $374,636.18 (a reduction of 51.5% and 9.4% in comparison with Scenarios 1 and 2, respectively). The integration of DG in Scenario 2 drastically cuts grid purchasing costs by 86.9% in comparison with Scenario 1. Furthermore, Scenario 3 demonstrates the efficiency of Demand Response (DR). Although incurring a $19,139.63 load adjustment cost, the DR program facilitates a 72.9% reduction in grid purchasing costs compared to Scenario 2 (dropping to $26,330.55). Additionally, the local support from DG units in Scenarios 2 and 3 helps relieve network congestion, thereby halving the annualized conductor investment cost in comparison with Scenario 1.

The optimal conductor cross-sections determined for each scenario are listed in Table 5. A significant reduction in conductor sizing is observed when transitioning from Scenario 1 to Scenarios 2 and 3. In Scenario 1, the absence of DG requires the grid to supply the total demand, necessitating large conductors at the beginning of the feeder to withstand high current flows (branches 1 and 2 require type k20). Conversely, in Scenarios 2 and 3, the integration of distributed generation supplies power locally, thereby relieving current congestion in the main feeders. Consequently, the optimization algorithm selects significantly smaller conductors for the same branches (downsizing to k5 for branch 1).

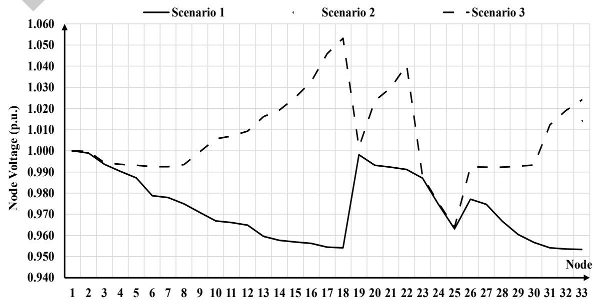

Fig. 6. Comparison of nodal voltages among scenarios at t = 20

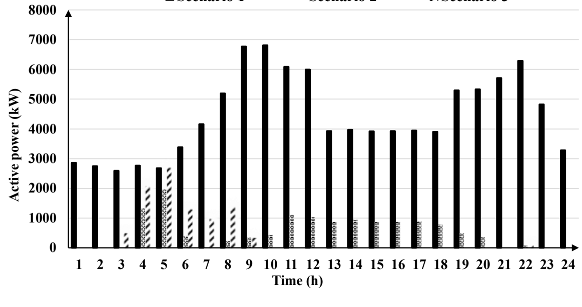

Fig. 7. Power purchased from the transmission grid

While most branches exhibit this downsizing trend, a few downstream branches (22–24 and 32) maintain identical cross-sections across all scenarios, as they carry lighter loads unaffected by upstream power-flow changes. This substantial reduction in conductor sizes in Scenarios 2 and 3 directly explains the 50% saving in annualized investment costs previously analyzed in Table 4.

Fig. 5 illustrates the daily voltage profile at bus 11 across the three scenarios. The results highlight the dominant role of distributed generation in voltage support compared to demand response. In Scenario 1, despite the implementation of load adjustment, the voltage profile remains consistently low, fluctuating between 0.9554 p.u. and 0.9833 p.u. throughout the day. This indicates that without the real and reactive power injection from local DG units, relying solely on DR is insufficient to boost the nodal voltage to the nominal level (1.0 p.u.). In contrast, the integration of DG in Scenarios 2 and 3 significantly elevates the voltage profiles during the main operating hours (t = 7–24), maintaining magnitudes close to 1.0–1.01 p.u. However, a notable phenomenon occurs at t = 5, where Scenario 3 exhibits the deepest voltage dip (0.9532 p.u.), even lower than Scenario 2 (0.9692 p.u.). This behavior is a direct consequence of the demand response strategy in Scenario 3. To minimize operating costs, the optimization algorithm shifts a significant amount of flexible load to this off-peak hour (t = 5). The resulting concentration of load demand causes a temporary voltage sag. Nevertheless, this value remains within the permissible limits, demonstrating that the system successfully trades off a slight voltage margin for optimal economic efficiency.

Fig. 6 details the nodal voltage profiles at t = 20. The comparison reveals a fundamental difference in network behavior. In Scenario 1, the network exhibits a typical radial voltage drop profile, decreasing continuously from the slack bus (Bus 1) to the remote ends. Consequently, the voltage at downstream nodes drops significantly, reaching a minimum of 0.9534 p.u. at node 33. Conversely, Scenarios 2 and 3 demonstrate the voltage support capability of distributed generation. Instead of a monotonic drop, the voltage profiles rise significantly at specific locations, particularly peaking at bus 18. This local voltage rise (reaching 1.0413 p.u. in Scenario 2 and 1.0532 p.u. in Scenario 3) is directly attributed to the real power injection from the DG unit installed at this bus. Furthermore, Scenario 3 outperforms Scenario 2, maintaining higher voltage levels across most nodes (e.g., at Bus 33, voltage improves to 0.9638 p.u. vs. 0.9634 p.u.). This improvement implies that the demand response program effectively reduced or shifted the peak load during this hour, thereby alleviating network stress and working in coordination with DGs to maintain an optimal voltage profile.

Table 5. Comparison of optimal conductor cross-sections among the three scenarios

Branch	**Scenario**			**Branch**	**Scenario**			**Branch**	**Scenario**		
	1	2	3		1	2	3		1	2	3
1	k20	k5	k5	12	k8	k4	k6	23	k2	k2	k2
2	k20	k7	k5	13	k8	k5	k5	24	k1	k1	k1
3	k18	k3	k3	14	k2	k5	k5	25	k8	k2	k2
4	k18	k4	k3	15	k2	k5	k5	26	k8	k2	k2
5	k15	k5	k3	16	k1	k5	k5	27	k8	k2	k2
6	k14	k2	k3	17	k1	k5	k5	28	k8	k2	k2
7	k14	k2	k3	18	k1	k2	k2	29	k8	k2	k2
8	k8	k4	k4	19	k1	k2	k2	30	k4	k1	k1
9	k8	k4	k4	20	k1	k2	k2	31	k3	k1	k1
10	k8	k4	k4	21	k1	k2	k2	32	k2	k2	k2
11	k8	k4	k4	22	k2	k2	k2				

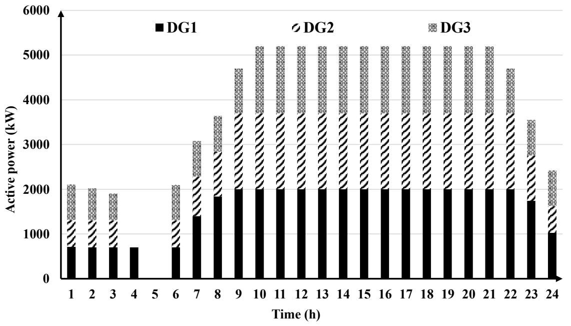

Fig. 8. Active power output of DG units in Scenario 2

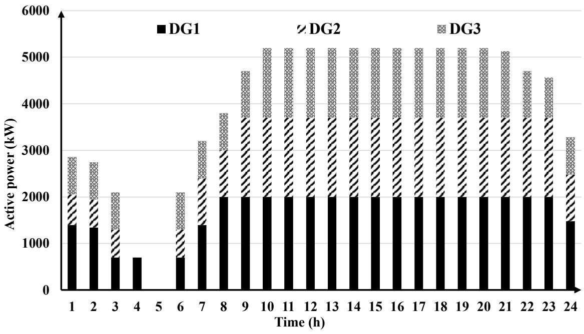

Fig. 9. Active power output of DG units in Scenario 3

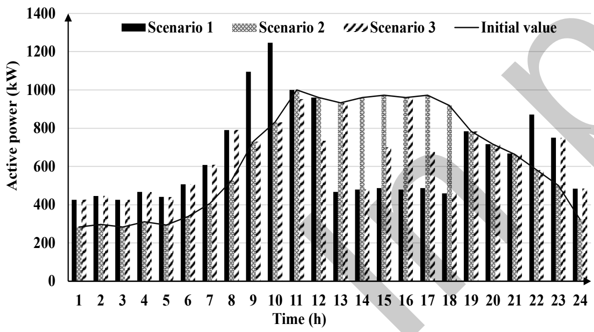

Fig. 10. Load power profile at bus 8 under the load adjustment scheme

Fig. 7 describes the power transactions profile between the distribution system and the transmission network over 24 hours. Here, positive values signify power purchases from the upstream grid (import), while negative values indicate power sales to the grid (export). In Scenario 1, the network imports power from the external grid throughout the entire day, with a peak import of 6,809.34 kW at t = 10. Conversely, Scenarios 2 and 3 show a reduced dependency on the external grid due to the contribution of distributed generation. Specifically, Scenario 2 draws power from the grid during the interval t = 3–9, whereas Scenario 3 imports power from t = 4 to t = 20. The maximum purchasing power for both Scenarios 2 and 3 occurs at t = 5, reaching 1,967.37 kW and 2,674.97 kW, respectively.

Fig. 8 and Fig. 9 illustrate the power purchased from distributed generation (DG) units in Scenario 2 and Scenario 3. The power purchased from DG units in these two scenarios differs during the periods from t = 1 to t = 3 and from t = 23 to t = 24, due to the integration of adjustable loads in Scenario 3. Furthermore, at t = 5, no power is purchased by the network from DG units in either scenario. This can be attributed to the fact that the electricity price is at its lowest at this specific time; therefore, the network prioritizes purchasing power from the external grid to take advantage of the cost benefit.

Fig. 10 depicts the load power profile at bus 8 under the load adjustment scheme. Since Scenario 2 does not incorporate adjustable loads, the load demand remains at its initial consumption level. Both Scenario 1 and Scenario 3 exhibit upward and downward power adjustments at bus 8; however, they differ in terms of the initiation timing and adjustment magnitudes at specific time instances.

In scenario 1:

− The load at bus 8 undergoes power reduction during t = 13–18. Within the interval from t = 13 to t = 18, the maximum power reduction reaches 50% of the initial demand.

− The load at bus 8 increases during the periods from t = 1 to t = 10 and from t = 22 to t = 24, with the maximum upward adjustment in all hours reaching 50% of the initial demand.

− During the remaining intervals, the load maintains its initial power consumption level.

In scenario 3:

− The load at bus 8 reduces power during the period of time from t = 11 to t = 18, with a maximum reduction of 50% of the initial demand at t = 18 and a minimum reduction of 4.79% at t = 11.

− The load at bus 8 increases power during the periods from t = 1 to t = 8 and from t = 23 to t = 24. Within the intervals from t = 1 to t = 10 and from t = 22 to t = 24, the maximum upward power adjustment consistently equals 50% of the initial demand.

− During the remaining intervals, the load maintains its initial power consumption level.

4. Conclusions

This study develops an optimization model to determine the optimal conductor cross-sections in distribution systems, accounting for the integration of distributed generation and shiftable loads. The objective function aims to minimize the total annualized expense of the grid, which encompasses capital and maintenance expenditures for conductors, energy procurement costs from the main grid, DG power purchase costs, and expenses related to load adjustments. The optimization framework is developed as a mixed-integer linear programming problem. The proposed optimization model is validated on a modified IEEE 33-bus system across three distinct scenarios using the GUROBI commercial solver and the GAMS programming language. Numerical results demonstrate that the coordinated scenario involving both DG and shiftable loads achieves the minimum cost, whereas the scenario considering only shiftable loads without DG integration results in the highest system cost. Consequently, the simultaneous integration of distributed generation and shiftable loads proves highly effective for the optimal selection of conductor sizes in distribution networks. Future research will aim to validate the proposed MILP model and optimization framework using real-world case studies and large-scale distribution networks to further assess its practical feasibility.

Acknowledgments

This work was supported by the Hanoi University of Science and Technology (HUST) under the Grant T2024-PC-065.

References

[1] V. Farahani, S. H. H. Sadeghi, H. A. Abyaneh, S. M. M. Agah, and K. Mazlumi, Energy loss reduction by conductor replacement and capacitor placement in distribution systems, IEEE Transactions Power Systems, vol. 28, iss. 3, pp. 2077–2085, Aug. 2013. https://doi.org/10.1109/TPWRS.2013.2251012

[2] H. Ali, S. Ullah, I. Sami, N. Ahmad, and F. Khan, Economic loss minimization of a distribution feeder and selection of optimum conductor for voltage profile improvement, in 2018 International Conference on Power Generation Systems and Renewable Energy Technologies (PGSRET*)*, pp. 1–6, Sep. 2018. https://doi.org/10.1109/PGSRET.2018.8686040

[3] B. R. Meier and B. Chowdhury, A Simple approach to conductor sizing and prolonging the thermal life of electrical cables below 1000 v for industrial and commercial applications, IEEE Transactions on Industry Applications, vol. 55, iss. 5, pp. 4507–4514, Sep. 2019. https://doi.org/10.1109/TIA.2019.2928238

[4] J. F. Franco, M. J. Rider, M. Lavorato, and R. Romero, Optimal conductor size selection and reconductoring in radial distribution systems using a mixed-integer LP approach, IEEE Transactions on Power Systems, vol. 28, iss. 1, pp. 10–20, Feb. 2013. https://doi.org/10.1109/TPWRS.2012.2201263

[5] A. D. Taslimov, M. V. Melikuziev, A. M. Najimova, and A. A. Alimov, Economic load intervals for selection of cable sections for agricultural purpose, E3S Web of Conferences, vol. 216, p. 01159, 2020. https://doi.org/10.1051/e3sconf/202021601159

[6] A. Rastgou, S. Bahramara, and J. Moshtagh, Flexible and robust distribution network expansion planning in the presence of distributed generators: Flexible and robust distribution network expansion planning in the presence of distributed generators, International Transactions on Electrical Energy Systems, vol. 28, iss. 12, p. e2637, Dec. 2018, https://doi.org/10.1002/etep.2637

[7] S. M. Ismael, S. H. E. A. Aleem, A. Y. Abdelaziz, and A. F. Zobaa, Practical considerations for optimal conductor reinforcement and hosting capacity enhancement in radial distribution systems, IEEE Access, vol. Vol. 6, pp. 27268–27277, May. 2018, https://doi.org/10.1109/ACCESS.2018.2835165

[8] M. A. Farrag, A. H. Khalil, and S. Omran, Optimal conductor selection and capacitor placement in radial distribution system using nonlinear AC load flow equations and dynamic load model, International Transactions on Electrical Energ Systems, vol. 30, iss. 5, Feb. 2020. https://doi.org/10.1002/2050-7038.12316

[9] O. Montoya Giraldo, A. Garces, and C. Castro, Optimal conductor size selection in radial distribution networks using a mixed-integer non-linear programming formulation, IEEE Latin America Transactions, vol. 16, iss. 8, pp. 2213–2220, Aug. 2018. https://doi.org/10.1109/TLA.2018.8528237

[10] R. S. Rao, K. Satish, and S. V. L. Narasimham, Optimal conductor size selection in distribution systems using the harmony search algorithm with a differential operator, Electric Power Components and Systems - ELECTR POWER COMPON SYST, vol. 40, iss. 1, pp. 41–56, Nov. 2011. https://doi.org/10.1080/15325008.2011.621922

[11] N. V. Pham, T. H. T. Nguyen, V. Y. Pham, and H. N. Nguyen, Using simplified distflow-based mixed-integer quadratically constrained programming formulation for optimum selection of conductor size in electrical distribution networks, Journal of Electrical Systems , vol. 20, no. 2, pp. 1497–1511, Apr. 2024. https://doi.org/10.52783/jes.1453

[12] N.-V. Pham and C.-C. Pham, A MISOCP-based methodology for optimally selecting conductor cross-sections in electricity distribution grids considering daily patterns and voltage-dependence of loads, Engineering Research Express, vol. 8, iss. 6, Mar. 2026, Art. no. 065320. https://doi.org/10.1088/2631-8695/ae4f5e

[13] J. A. Guzmán-Henao, B. Cortés-Caicedo, R. I. Bolaños, L. F. Grisales-Noreña, and O. D. Montoya, Optimal conductor selection and phase balancing in three-phase distribution systems: An integrative approach, *Results in Engineering*, vol. 24, p. 103416, Dec. 2024. https://doi.org/10.1016/j.rineng.2024.103416

[14] V. Zdraveski and M. Todorovski, Conductor size selection in radial distribution networks using robust optimization, Sustainable Energy, Grids and Networks, vol. 43, Sep. 2025, Arrt. No. 101730. https://doi.org/10.1016/j.segan.2025.101730

[15] L. A. Gallego Pareja, J. M. López-Lezama, and O. Gómez Carmona, Optimal Integration of Distribution Network Reconfiguration and Conductor Selection in Power Distribution Systems via MILP, *Energies*, vol. 16, iss. 19, p. 6998, Oct. 2023, https://doi.org/10.3390/en16196998

[16] Y. Wu, M. Barati, and G. J. Lim, A Pool strategy of microgrid in power distribution electricity market, IEEE Transactions on Power Systems., vol. 35, iss. 1, pp. 3–12, Jan. 2020. https://doi.org/10.1109/TPWRS.2019.2916144

[17] L. Bai, J. Wang, C. Wang, C. Chen, and F. Li, Distribution locational marginal pricing (dlmp) for congestion management and voltage support, IEEE Transactions on Power Systems., vol. 33, iss. 4, pp. 4061–4073, Jul. 2018. https://doi.org/10.1109/TPWRS.2017.2767632

[18] S. Wang, S. Chen, L. Ge, and L. Wu, Distributed generation hosting capacity evaluation for distribution systems considering the robust optimal operation of OLTC and SVC, IEEE Transactions on Sustainable Energy, vol. 7, iss. 3, pp. 1111–1123, Jul. 2016. https://doi.org/10.1109/TSTE.2016.2529627

[19] Y. Li, Q. Chen, G. Strbac, K. Hur, and C. Kang, Active distribution network expansion planning with dynamic thermal rating of underground cables and transformers, IEEE Transactions on Smart Grid, vol. 15, iss. 1, pp. 218–232, Jan. 2024. https://doi.org/10.1109/TSG.2023.3266782

[20] C. Ge, S. Lin, F. Li, P. Wang, F. Yang, and D. Li, Optimal coordination method for an ADN with multiple network-constrained VPPs, IEEE Transactions on Power Systems,. vol. 40, iss. 1, pp. 394–407, Jan. 2025. https://doi.org/10.1109/TPWRS.2024.3398019

[21] S. H. Dolatabadi, M. Ghorbanian, P. Siano, and N. D. Hatziargyriou, An Enhanced IEEE 33 bus benchmark test system for distribution system studies, IEEE Transactions on Power Systems., vol. 36, iss. 3, pp. 2565–2572, May 2021. https://doi.org/10.1109/TPWRS.2020.3038030

[22] GAMS Documentation 46, (Feb. 17, 2024). GAMS Development Corp. Accessed: Feb. 25, 2026. [Online]. Available: https://www.gams.com

[23] S. M. Ismael, S. H. E. Abdel Aleem, A. Y. Abdelaziz, and A. F. Zobaa, Optimal conductor selection of radial distribution feeders: an overview and new application using grasshopper optimization algorithm, in Classical and Recent Aspects of Power System Optimization, Elsevier, 2018, pp. 185–217. https://doi.org/10.1016/B978-0-12-812441-3.00008-2

[24] W. A. Bukhsh, C. Zhang, and P. Pinson, An Integrated multiperiod opf model with demand response and renewable generation uncertainty, IEEE Transactions on Smart Grid, vol. 7, iss. 3, pp. 1495–1503, May 2016. https://doi.org/10.1109/TSG.2015.2502723

[25] M. R. Dorostkar-Ghamsari, M. Fotuhi-Firuzabad, M. Lehtonen, and A. Safdarian, Value of distribution network reconfiguration in presence of renewable energy resources, IEEE Transactions on Power Systems., vol. 31, iss. 3, pp. 1879–1888, May 2016. https://doi.org/10.1109/TPWRS.2015.2457954

[26] S. S. F. Souza, R. Romero, J. Pereira, and J. T. Saraiva, Artificial immune algorithm applied to distribution system reconfiguration with variable demand, International Journal of Electrical Power & Energy Systems, vol. 82, pp. 561–568, Nov. 2016. https://doi.org/10.1016/j.ijepes.2016.04.038

[27] L. Bai, J. Wang, C. Wang, C. Chen, and F. Li, Distribution Locational Marginal Pricing (DLMP) for Congestion Management and Voltage Support, IEEE Transactions on Power Systems., vol. 33, iss. 4, pp. 4061–4073, Jul. 2018. https://doi.org/10.1109/TPWRS.2017.2767632